Heliyon 8 (2022) e10045

Contents lists available at ScienceDirect

Heliyon

journal homepage: www.cell.com/heliyon

Research article

A flexible luminescence film with temperature and infrared response based on Eu^{2+}/Dy^{3+} co-doped $Sr_2Si_5N_8$ phosphors for optical information storage applications

Hao Song [a,1], Xiuping Wu [b,1], Yanjie Zhang [a,b,**], Shichang Xu [a], Bing Li [b,*]

[a] Research Institute of Photonics, Dalian Polytechnic University, Dalian 116034, China
[b] Shanxi Province Key Laboratory of Oral Diseases Prevention and New Materials, Shanxi Medical University, Taiyuan 030001, China

ARTICLE INFO

Keywords:
Advanced optical materials
$Sr_2Si_5N_8$
Trap engineering
Optical information storage

ABSTRACT

Deep-trap luminescent materials have attracted great attention for optical information storage applications. However, the flexible luminescence films based on red luminescence materials with temperature and infrared response are scarce. In this study, we have successfully developed various novel flexible red emitting films based on Eu^{2+}/Dy^{3+} co-doped $Sr_2Si_5N_8$ phosphors through screen-printing and spin-coating technologies, respectively. Interestingly, the fabricated flexible luminescence films exhibit unique temperature and infrared responsive properties for optical information storage by releasing photons in response to thermal or infrared stimulation. Notably, deep-trap red emitting Eu^{2+}/Dy^{3+} co-doped $Sr_2Si_5N_8$ phosphors are crucial for the optical information storage properties of the films. Two emission peaks of $Sr_2Si_5N_8:Dy^{3+}$ phosphors at 476 nm and 577 nm are observed under excitation at 345 nm, corresponding to the radiative transition occurs from the $^4F_{9/2}$ level to the $^6H_{13/2}$ and $^6H_{15/2}$ levels of Dy^{3+}. When Dy^{3+} and Eu^{2+} ions are co-doped in $Sr_2Si_5N_8$, the energy transfer from Dy^{3+} to Eu^{2+} in $Sr_2Si_5N_8$ matrix is found and the decay time confirms that Dy^{3+} ions can be acted as deep trap centers to storage photons. For $Sr_2Si_5N_8:Eu^{2+},Dy^{3+}$ phosphors and the corresponding flexible luminescence films, the specific patterns (for example apple and note patterns) are firstly recorded under NUV or blue light excitation and then reappear through thermal stimulation or near-infrared photo-stimulation (980 nm laser). This work not only validates the feasibility of $Sr_2Si_5N_8:Eu^{2+},Dy^{3+}$ phosphors as deep-trap red emitting luminescence materials, but also suggests the applications of flexible luminescence films for optical information storage.

1. Introduction

Optical information storage has received much attention in modern information storage fields due to its energy saving, fast response speed, high efficiency and environmental-friendliness [1, 2]. Compared with the traditional optical information storage technologies, the novel full-color optical information storage technology based on advanced optical materials has been developed [3, 4, 5, 6, 7]. A series of deep-trap green-emitting and blue-emitting luminescence materials such as Eu^{2+}/Dy^{3+}-doped $SrSi_2O_2N_2$ system and $BaSiO_3:Eu^{2+}$ were designed and exhibited its application in information storage [8, 9, 10, 11]. However, the lack of suitable red-emitting luminescence material is the bottleneck for full-color anti-counterfeiting optical information storage technology owing to the requirement of three primary colors (RGB) [12, 13]. Until now, it is still a great challenge to develop red persistent luminescence materials and their corresponding devices for the application of full-color anti-counterfeiting optical information storage and medical imaging [14].

Recently, great efforts have been focused on developing red-emitting phosphors for white light emitting diodes (LEDs) [15, 16, 17, 18]. Among them, nitride phosphors with M-Si-N (M = Ca, Sr or Ba) framework are regarded as the potential red-emitting phosphors for white LEDs because of their high efficiency, low thermal quenching and excellent chemical stability [19, 20, 21, 22, 23]. As a member of nitride phosphors, $Sr_2Si_5N_8:Eu^{2+}$ phosphor exhibits intense red emission at 600–650 nm excited by near UV and blue LEDs, ascribing to the rigid framework built by the SiN_4 tetrahedra to form a three-dimensional network through

* Corresponding author.
** Corresponding author.
E-mail addresses: zhang_yj@dlpu.edu.cn (Y. Zhang), libing-1975@163.com (B. Li).
[1] These authors contributed equally and served as co-first authors.

https://doi.org/10.1016/j.heliyon.2022.e10045
Received 24 June 2022; Received in revised form 2 July 2022; Accepted 19 July 2022

corner-sharing N atoms [24, 25, 26]. In past decades, the researches were focused on preparation methods of $Sr_2Si_5N_8:Eu^{2+}$ phosphor and various synthetic methods have been found, e.g. traditional solid state reaction, carbothermal reduction and nitridation, gas nitridation under high pressure, sol-gel-nitridation, pellet method [24, 27, 28, 29, 30]. However, it is quite essential to find suitable deep-trap centers and thoroughly study their photoluminescence properties for red-emitting persistent $Sr_2Si_5N_8$ based nitride phosphors. As for red persistent phosphors, Eu^{2+} doped sulfides and oxysulfides encounter the problems of low chemical stability, moisture sensitivity and harmful S for the environment. The $Ca_2Si_5N_8:Eu^{2+},Tm^{3+}$ phosphors can be a promising candidate for reddish-orange long-lasting luminescence material [31, 32]. $Sr_2Si_5N_8:Eu^{2+},Dy^{3+}$ red phosphor has been prepared by sol-gel-nitridation method for white light emitting diodes [24]. However, the energy transfer mechanism and red luminescence properties with temperature and infrared response for $Sr_2Si_5N_8$ phosphors are scarcely discussed. More importantly, the design and development of flexible luminescence films based on polydimethylsiloxane (PDMS) and polypropylene (PP) play a crucial role in expanding application of optical information storage [33, 34]. Therefore, the simple and efficient method to prepare flexible luminescence film with temperature and infrared response is highly desirable.

Herein, a series of flexible luminescence films with red emitting $Sr_2Si_5N_8:Eu^{2+},Dy^{3+}$ phosphors are newly fabricated by screen-printing and spin-coating technologies. Excitingly, the luminescence films exhibit excellent thermal and infrared stimulated luminescence properties for optical information storage applications (write in by NUV or blue light and read out by temperature or near-infrared light). The $Sr_2Si_5N_8:Dy^{3+}$ phosphor has two emission peaks at 577 nm and 480 nm excited by 345 nm and Dy^{3+} ions can act as deep trap center in $Sr_2Si_5N_8:Eu^{2+},Dy^{3+}$ phosphors to increase the storage capacity of the red emitting phosphor. Moreover, the energy transfer mechanism from Dy^{3+} ions to Eu^{2+} ions is discussed in detail. The results suggest that $Sr_2Si_5N_8:Eu^{2+},Dy^{3+}$ phosphors and the corresponding flexible luminescence films play critical roles of the potential applications in full-color optical information storage.

2. Experimental section

2.1. Synthesis of $Sr_2Si_5N_8:Eu^{2+},Dy^{3+}$ phosphors

All $Sr_{2-x-y}Si_5N_8:xEu^{2+},yDy^{3+}$ (denoted as SSN:xEu^{2+},yDy^{3+}) powders were synthesized from the raw materials of $SrCO_3$ (A.R., Aladdin, China), Si_3N_4 (SN-E10, UBE Industries, Tokyo), Eu_2O_3 (99.99 %, Aladdin, China), Dy_2O_3 (99.99 %, Aladdin, China) and $C_3H_6N_6$ (A.R., Aladdin, China). In this case, $C_3H_6N_6$ was doped as a reducing agent in a ratio of 1.5 M ratio of C/Sr. The stoichiometrically weighted raw materials were mixed thoroughly in an agate mortar. The mixtures were placed in molybdenum crucibles and calcined in a high temperature tubular furnace at 1600 °C for 9 h under 3 % H_2/N_2 atmosphere (150 mL/min). After cooling down naturally, the samples were reground and washed with deionized water for subsequent characterization.

2.2. Fabrication of flexible luminescence films

Fabrication of flexible luminescence films by spin-coating and screen-printing process is shown in Figure 1. The synthesized samples were firstly mixed with polydimethylsiloxane (PDMS) resin precursors (in liquid) and firming agent (1:1) in a mass content of 20 % under stirring. In a typical spin-coating process, the phosphor slurries were cast on smooth glass substrate and a flexible luminescence film with the thickness of ~0.4 mm was completely peeled off the glass with the help of a blade after curing at 80 °C for 2 h. For the screen-printing process (Figure 1), the phosphor slurries with 20 wt% content were manually printed on the surface of polypropylene polymer (PP) using a 200-mesh screen. Then, the flexible luminescence film based on PP was obtained after sintering at 130 °C for 3 h.

2.3. Characterization

Phase identification and crystal structure analysis of the samples were characterized by X-ray di-ractometer (XRD, Shimadzu, XRD-7000s) with Cu Kα radiation (0.15374 nm) operating at 40 kV and 20 mA in a 2θ range from 10° to 70° at scanning speed of 5° per minute. The morphology and particle sizes were investigated by field emission electron microscope (FESEM, JSM-7800F, JEOL). The photoluminescence excitation (PLE) and emission (PL) spectra were measured using fluorescence spectrophotometer (Hitachi, F-7000) equipped with a 200 W Xe lamp as excitation source at room temperature. The decay time curves of the as-synthesized samples excited by 345 nm and monitored at 476 nm were determined by fluorescence spectrophotometer (FLS920, Edinburgh Instruments Ltd.) equipped with a steady-state xenon lamp as excitation source (Xe900, 450 W). Thermoluminescence (TL) curve was recorded from RT to 350 °C using an SL08-L thermoluminescence dosimeter with a heating rate of 2 °C s^{-1} (sample was pre-irradiated with 254 nm UV for 5 min and then held in the dark for 5 min). Temperature-dependent photoluminescence properties were recorded at 370 nm excitation by a spectrometer equipped with an Oxford instruments liquid nitrogen thermostat (FLS920, Edinburgh Instruments Ltd.) with a dwell time of 10 min at each temperature point.

2.4. Optical information write-in and readout

The flexible luminescence films were covered by a photomask with specific photographic patterns and excited for 3 min by ultraviolet light (254 nm). After removing the UV excitation light and photomask, the specific photographic pattern information was recorded in the luminescence films. It was found that the specific photographic pattern was

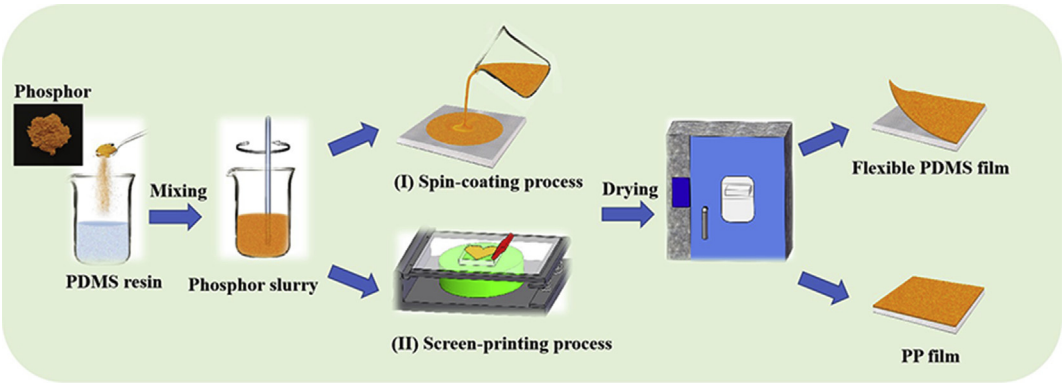

Figure 1. Schematic diagram for fabrication of flexible luminescence films by spin-coating and screen-printing process.

integrally retrieved when the luminescence films were heated to target temperature (~100 °C or 200 °C). Moreover, the optical information readout was also achieved using a 980 nm laser (200 mW) as excitation source for the luminescence films.

3. Results and discussion

3.1. Phase identification and microstructure analysis

The powder XRD patterns of the as-synthesized phosphors are recorded to identify the phase purity. In Figure 2a, the XRD patterns of SSN:0.02Dy^{3+}, SSN:0.02Eu^{2+},0.02 Dy^{3+} and SSN:0.05Eu^{2+} samples match well with standard data (PDF card no. 85-0101) of $Sr_2Si_5N_8$ crystal. All samples doped with Dy^{3+} and Eu^{2+} ions correspond to the orthorhombic crystal lattice with the space group of $Pmn2_1$. Clearly, no other impurity phases (*e.g.* Dy_2O_3 and Eu_2O_3) can be found, which indicates that Dy^{3+} and Eu^{2+} ions can be effectively incorporated into $Sr_2Si_5N_8$ host lattice.

Figure 2b exhibits the crystal structure of $Sr_2Si_5N_8$ based on a typical corner sharing structure. There are at two different crystallographic sites with eight (Sr_I) and nine (Sr_{II}) nitrogen coordinates for Sr atoms in $Sr_2Si_5N_8$ lattices. The ionic radii of Sr^{2+} ions with eight and nine coordinates are 1.28 Å and 1.33 Å, respectively. The similar ionic radii of Eu^{2+} ions (1.25 Å for eight coordinate and 1.30 Å for nine coordinate) with Sr^{2+} ions facilitate the substitution in host lattice and result in the same diffraction peak in XRD patterns. The ionic radii of Dy^{3+} ions are 1.027 Å for eight coordinate and 1.083 Å for nine coordinates. Thus, Dy^{3+} ions can randomly substitute Sr_I and Sr_{II} sites in $Sr_2Si_5N_8$ crystal due to the smaller radius than Sr^{2+} ions, which will great influence the characteristic photoluminescence properties of Dy^{3+} ions in $Sr_2Si_5N_8$ host.

FE-SEM micrographs of $Sr_2Si_5N_8$:0.02Eu^{2+},0.02Dy^{3+} phosphors are depicted to investigate the morphology and particle sizes in Figure 2c. The SSN:0.02Eu^{2+},0.02Dy^{3+} phosphor exhibits smooth and irregular morphology with particle sizes of ~1–10 μm. Obviously, the powders are aggregated by the smaller grain-like particles with ~100–200 nm in diameter.

In order to further verify the position of the $Eu^{2+}$and Dy^{3+} ions substitution, the XRD data of the $Sr_2Si_5N_8$:0.02Eu^{2+},0.02Dy^{3+} sample is refined by Rietveld to obtain detailed crystal information. It is worth indicating that the diffraction peaks of a very small number of impurity phases are removed prior to refinement for the accuracy of the refinement data. Figure 3 shows the Rietveld refinement of the $Sr_2Si_5N_8$:0.02-Eu^{2+},0.02Dy^{3+} sample and the obtained structural parameters are listed in Table 1. The optimized reliability factors are R_{wp} = 9.98 % and R_p = 5.62 %. The cell parameters are a = 5.7123 Å, b = 6.8103 Å, c = 9.3437 Å, V = 363.4917 $Å^3$, Z = 1.

3.2. Photoluminescence properties

The photoluminescence excitation and emission spectra of $Sr_{2-y}Si_5N_8$:yDy^{3+} (y = 0.005, 0.02, 0.04 and 0.05) phosphors are shown in Figure 4. In Figure 4a, the PLE spectra present a broad band ranging from 320 nm to 460 nm, ascribing to $^6H_{15/2} \rightarrow {}^6P_{7/2}$, $^6H_{15/2} \rightarrow {}^6P_{5/2}$, $^6H_{15/2} \rightarrow$

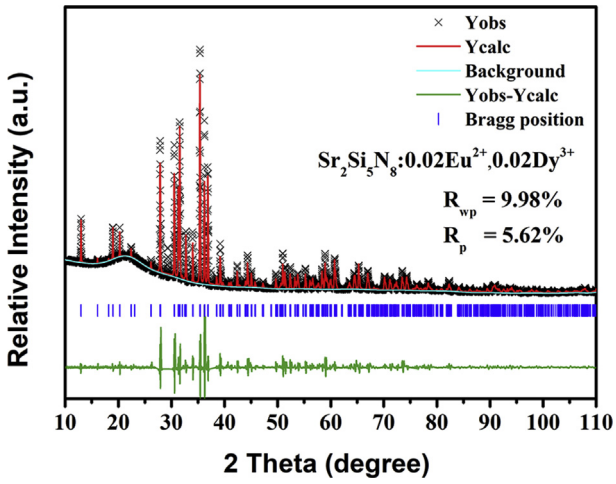

Figure 3. XRD Rietveld refinement of $Sr_2Si_5N_8$:0.02Eu^{2+},0.02Dy^{3+} sample.

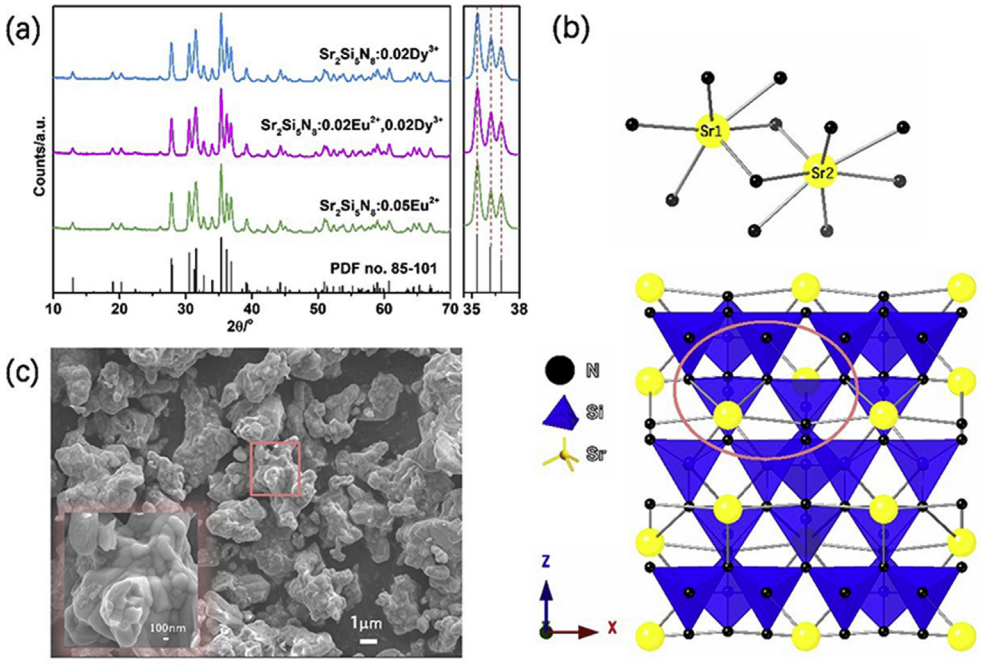

Figure 2. (a) XRD patterns of SSN:xEu^{2+},yDy^{3+} phosphors and standard card of $Sr_2Si_5N_8$ with PDF no. 85-101. (b) Crystal structure of $Sr_2Si_5N_8$. (c) FESEM images of SSN:0.02Eu^{2+},0.02Dy^{3+} phosphor prepared at 1600 °C for 9 h under a reducing atmosphere. Inset is high magnification image.

Table 1. Refined structure parameters of $Sr_2Si_5N_8$:0.02Eu^{2+},0.02Dy^{3+} derived from the Rietveld refinement.

Atom	Wyckoff position	x	y	z	Frac
Sr1	2a	0.0000	0.8736(8)	0.0010(6)	1
Sr2	2a	0.0000	0.8808(7)	0.3654(6)	1
Si1	4b	0.2511(12)	0.6685(8)	0.6861(24)	1
Si2	2a	0.0000	0.0542(11)	0.6858(36)	1
Si3	2a	0.0000	0.4291(20)	0.4663(14)	1
Si4	2a	0.0000	0.4039(16)	0.8998(10)	1
N1	2a	0.0000	0.1923(31)	0.5005(29)	1
N2	4b	0.2342(25)	0.9020(22)	0.6801(49)	1
N3	4b	0.2562(35)	0.4361(28)	0.0123(23)	1
N4	2a	0.0000	0.5818(46)	0.7757(26)	1
N5	2a	0.0000	0.1657(33)	0.8363(24)	1
N6	2a	0.0000	0.4304(39)	0.2774(26)	1

Cell parameters: a = 5.7123 Å, b = 6.8103 Å, c = 9.3437 Å, V = 363.4917 Å^3, Z = 1; space group: $Pmn2_1$; Reliability factors: R_{wp} = 9.98 %, R_p = 5.62 % and χ^2 = 8.269.

$^4I_{13/2}$, $^6H_{15/2}$ → $^4G_{11/2}$, $^6H_{15/2}$ → $^4I_{15/2}$ transitions of Dy^{3+} ions in $Sr_2Si_5N_8$ lattice. Under excitation of 345 nm, the PL spectra feature two broad emission peaks in blue region (465–508 nm) and yellow region (525–650 nm). The weak blue emission peaks are ascribed to the transitions of $^4F_{9/2}$ →$^6H_{15/2}$, which is the magnetic dipole transition. The strong yellow emission peaks can be found at 577 nm, attributed to the electric dipole transition of $^4F_{9/2}$ →$^6H_{13/2}$. The inset in Figure 4b displays the excitation spectra of SSN:0.04Dy^{3+} monitored at 485, 497 and 577 nm, respectively. Although the detected wavelength can only start from 300 nm due to the limitation of frequency peak, it can be found that the excitation band monitored at 577 nm shows a similar tendency with the one monitored at 485 nm. Thus, it can be deduced that the two broad emission peaks in Figure 4b originate from the transitions of Dy ions and the intensities of the strong yellow emission peaks are highly influenced by the crystal field surrounding the Dy^{3+} ions, which broadens the emission line of Dy^{3+} due to the Stark levels for the $^4F_{9/2}$ and ^6H_J levels [35, 36, 37, 38]. The crystal field strength of the Dy^{3+} ion plays a crucial role in the electric dipole transition. Moreover, the $^4F_{9/2}$ →$^6H_{13/2}$ transition belongs to a hypersensitive transition, which is a forced electric dipole transition being allowed only at low symmetry with no inversion center. Thus, the emission peaks at 577 nm and 588 nm are predominant because of the low-symmetry local sites and strong crystal field of Dy^{3+} ions in $Sr_2Si_5N_8$ lattice. The yellow emission peak intensity of SSN:yDy^{3+} phosphor at 577 nm increases obviously with the increase of Dy^{3+} doping concentration, and reaches the maximum value at y = 0.02. Then, the intensity of Dy^{3+} emission decreases for y = 0.04 and 0.05 due to the concentration quenching effect.

Figure 5 displays the PLE spectra (λ_{em} = 577 and 605 nm) and emission spectra (λ_{ex} = 345 nm) of the as-prepared SSN:0.02Dy^{3+}, SSN:0.02Eu^{2+}, SSN:0.02Eu^{2+},0.02Dy^{3+} phosphors. As can be seen in Figure 5a and 5b, the PLE spectrum of SSN:0.02Dy^{3+} shows a broad excitation band in the range of 320–460 nm when detected the emission peak at 577 nm and SSN:0.02Eu^{2+} phosphor exhibits a red emission centered at 620 nm under excitation of 370 nm. For SSN:0.02 Eu^{2+},0.02Dy^{3+} phosphor in Figure 5d, only red emission peak centered at 622 nm can be found owing to the $4f^65d^1$ - $4f^7$ transition of Eu^{2+} ions and the characteristic emissions of Dy^{3+} ions disappear even excited by 345 nm. The excitation spectrum of SSN:0.02 Eu^{2+} phosphor in Figure 5c consists of an ultra-wide band ranging from 320 nm to 520 nm with the dominant peak at 370 nm, overlapping the blue emission wavelengths of Dy^{3+} ions. Thus, it can be deduced that the energy transfer from Dy^{3+} ions to Eu^{2+} ions probably occur in the co-doped $Sr_2Si_5N_8$ phosphors.

In order to further investigate the photoluminescence improvement of the co-doped samples due to the energy transfer from Dy^{3+} to Eu^{2+}, the PL spectra of Dy^{3+} and Eu^{2+} co-doped $Sr_2Si_5N_8$ phosphors are conducted in Figure 6. As clearly indicated in Figure 6a, the red emission intensity for $Sr_2Si_5N_8$:0.02Eu^{2+},0.02Dy^{3+} phosphor is increased by 27 % under NUV excitation at 370 nm compared with $Sr_2Si_5N_8$:0.02Eu^{2+} phosphor, which probably originates from the energy transfer process between Dy^{3+} and Eu^{2+} ions. In Figure 6b, the PL intensity of $Sr_2Si_5N_8$:xEu^{2+},0.02Dy^{3+} phosphor increases gradually with the increase of Eu^{2+} concentration (x), and reaches to the maximum value at x = 0.02. Then, the PL intensity decreases to 95 % of the maximum value at x = 0.03 due to the concentration quenching effect. Moreover, it is obvious that emission wavelength of $Sr_2Si_5N_8$:xEu^{2+},0.02Dy^{3+} shifts from 616 nm to 629 nm with the increasing concentration of Eu^{2+}. This red-shift is related to an increase of the Stokes shift and possibly can also be attributed to some reabsorption by Eu^{2+} [23].

To further investigate the mechanism of energy transfer between Dy^{3+} and Eu^{2+}, the decay curves of $Sr_2Si_5N_8$:xEu^{2+},0.02Dy^{3+} (x = 0, 0.01, 0.02 and 0.05) phosphors excited at 345 nm and monitored at 476 nm are shown in Figure 7a-c. All curves can be fitted to a double exponential equation [39]:

$$I(t) = I_0 + A_1 exp(-t/\tau_1) + A_2 exp(-t/\tau_2) \quad (1)$$

where t is the time, $I(t)$ is the intensity at time t, I_0 is the background intensity (for very long times t), A_1 and A_2 are constants, τ_1 and τ_2 are rapid and slow lifetime for exponential components, respectively. The average decay time (τ^*) can be expressed as follows.

$$\tau^* = (A_1\tau_1^2 + A_2\tau_2^2)/(A_1\tau_1 + A_2\tau_2) \quad (2)$$

Based on Eqs. (1) and (2), the lifetime values of the phosphors are determined to be 64.15 μs, 1.46 μs, 0.09 μs and 0.15 μs for x = 0, 0.01, 0.02 and 0.05, respectively. Compared with Dy^{3+} singly-doped phosphor, the

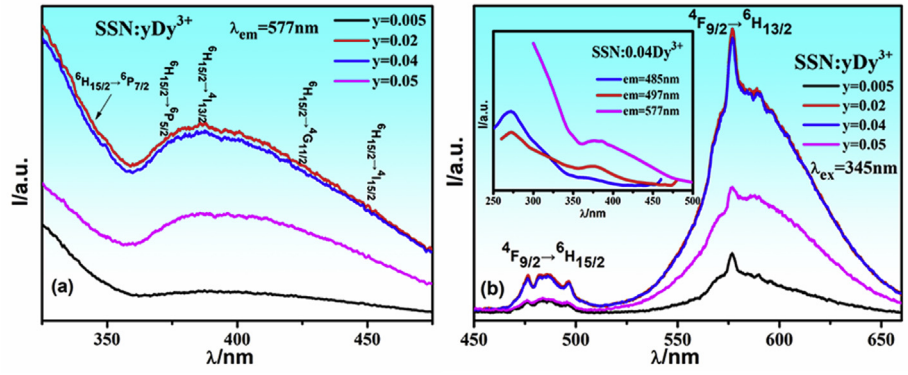

Figure 4. (a) Photoluminescence excitation and (b) emission spectra of $Sr_{2-y}Si_5N_8$:yDy^{3+} (y = 0.005, 0.02, 0.04 and 0.05) phosphors. The inset shows the excitation spectra of SSN:0.04Dy^{3+} monitored at 485, 497 and 577 nm, respectively.

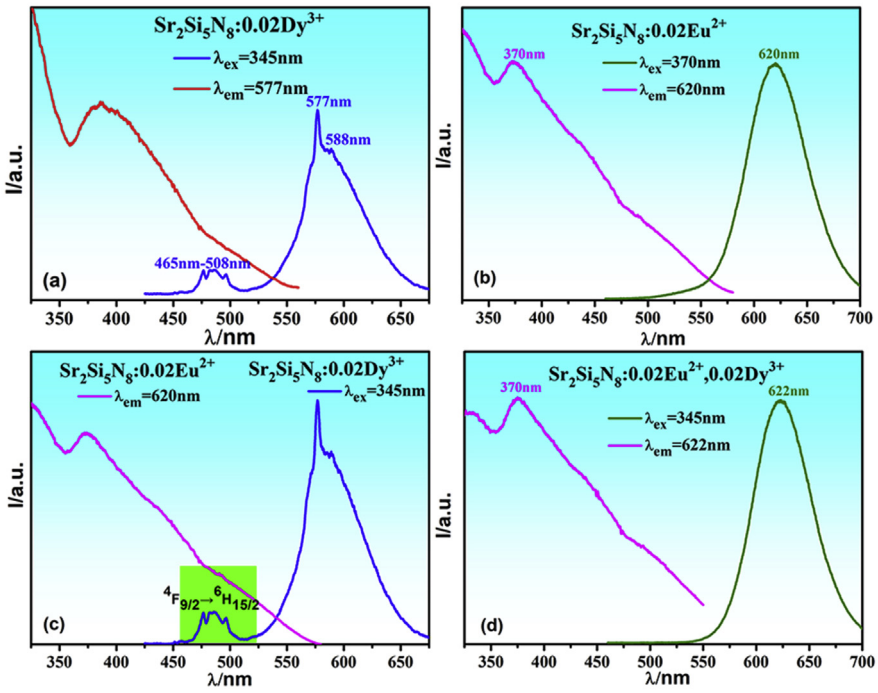

Figure 5. Excitation and emission spectra of the (a) SSN:0.02Dy^{3+} (λ_{em} = 577 nm; λ_{ex} = 345 nm) and (b) SSN:0.02Eu^{2+} (λ_{em} = 620 nm; λ_{ex} = 370 nm) phosphors. (c) Comparison of excitation spectra of SSN:0.02Eu^{2+} (λ_{em} = 620 nm) and emission spectra of SSN:0.02Dy^{3+} (λ_{ex} = 345 nm) phosphors, demonstrating the existence of spectral overlap. (d) Excitation and emission spectra of SSN:0.02Eu^{2+},0.02Dy^{3+} phosphors (λ_{em} = 622 nm; λ_{ex} = 345 nm).

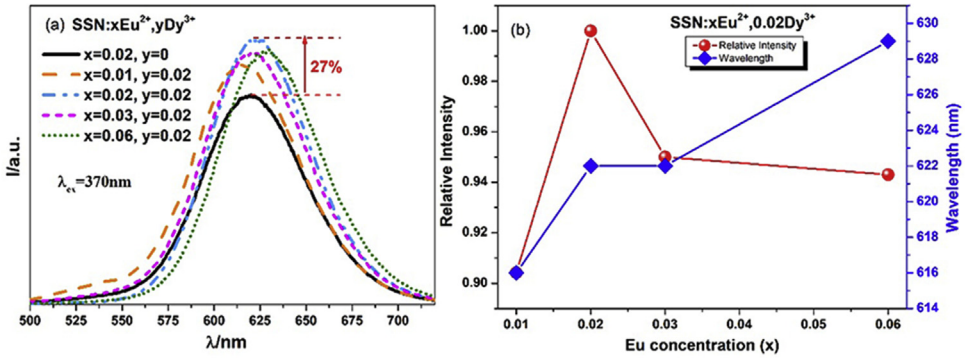

Figure 6. (a) PL spectra of Dy^{3+}/Eu^{2+} doped $Sr_2Si_5N_8$ phosphors with different concentration. (b) Relative intensity and wavelength variations of the phosphors as a function of Eu^{2+} concentration.

decay time of Dy^{3+} emission at 476 nm in co-doped samples greatly decreased from 64.15 μs (x = 0) to 0.09 μs (x = 0.02), which clearly demonstrates the energy transfer from Dy^{3+} ions to Eu^{2+} ions.

Currently, TL curve is a primary method to measure the trapping effect and their roles in the luminescent properties of phosphors. Figure 8 presents the normalized TL curves of $Sr_2Si_5N_8$:0.02Eu^{2+} and $Sr_2Si_5N_8$:0.02E-u^{2+},0.02Dy^{3+} phosphors at temperature variation (300–625 K). The trap depths are further estimated using the formulae, which are communicated as follows [40]:

$$E = T_m/500 \tag{3}$$

where E (eV) is the trap depth and T_m (K) is the temperature of the TL curve peaks. The TL curve peak for $Sr_2Si_5N_8$:0.02Eu^{2+} is confirmed as 360 K with the calculated trap depth of 0.72 eV by Eq. (3), which is probably attributed to the intrinsic traps from the equivalent substitution of Eu^{2+} for Sr^{2+} in SSN matrix. When Dy^{3+} is co-doped in SSN matrix, the TL curve shows two peaks with the strongest one at 408 K. The trap depths for $Sr_2Si_5N_8$:0.02Eu^{2+},0.02Dy^{3+} are calculated to be 0.656 eV (328 K) and 0.816 eV (408 K) by Eq. (3). These traps are $Dy_{Ba}^{\bullet}$ positive traps and V_{Sr}'' negative traps created by two Dy^{3+} ions substitutions for three Sr^{2+} ions when compensating for the excess positive charges generated by the nonequivalent substitution of Dy^{3+} for Sr^{2+}. Therefore, a reasonable co-doping of Dy^{3+} introduces a deeper trap for the material.

In the process of read out optical information, the phosphors usually require heating to 100 °C and above. Therefore, the thermal stability of phosphors is an important parameter in evaluating the performance of optical information storage materials. The temperature-dependent property of $Sr_2Si_5N_8$:0.02Eu^{2+},0.02Dy^{3+} phosphor is investigated by measuring the emission spectra at 25 °C, 50 °C, 100 °C and 150 °C, respectively. It is worth noting that the sample is dwelled at each temperature point for 10 min to avoid the TL emission before the emission spectra are measured. Figure 9a shows the variation of the PL spectra of $Sr_2Si_5N_8$:0.02Eu^{2+},0.02Dy^{3+} phosphor with temperature at 370 nm excitation. The variation of the relative emission intensity and the

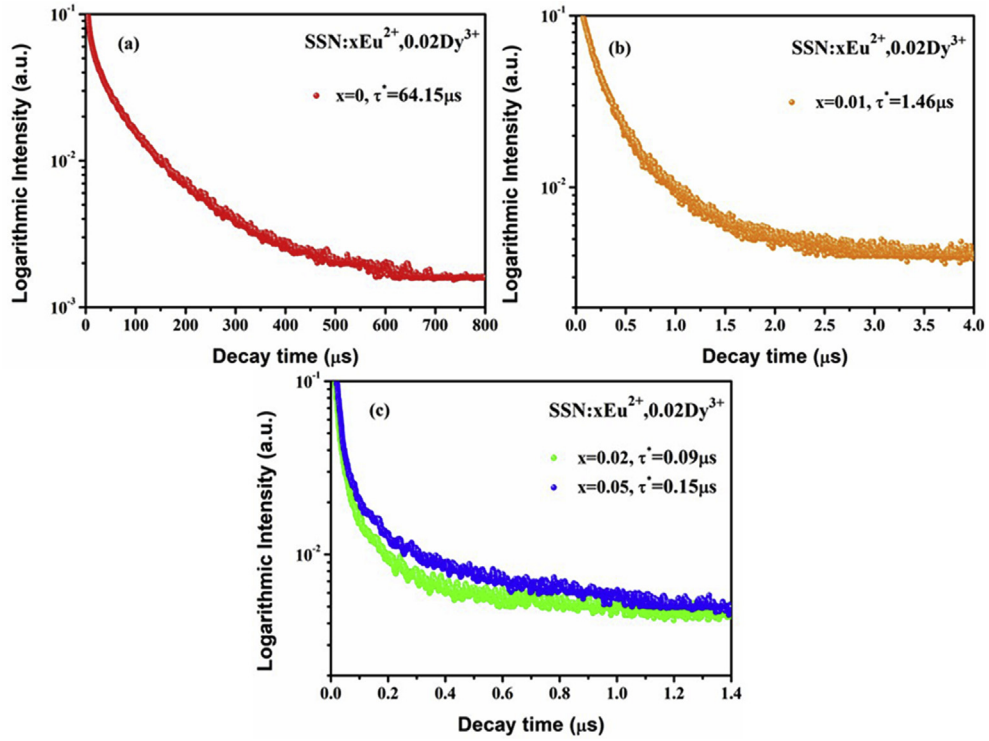

Figure 7. Decay curves of (a) $Sr_2Si_5N_8$:0.02Dy^{3+}, (b) $Sr_2Si_5N_8$:0.01Eu^{2+},0.02Dy^{3+}, (c) $Sr_2Si_5N_8$:0.02Eu^{2+},0.02Dy^{3+} and $Sr_2Si_5N_8$:0.05Eu^{2+},0.02Dy^{3+} phosphors excited by 345 nm and monitored at 476 nm.

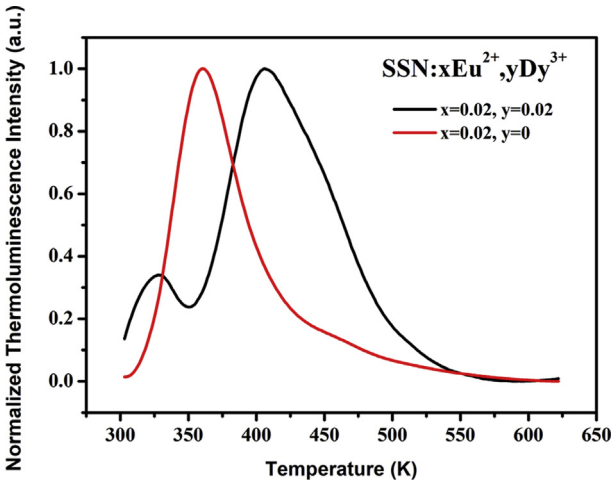

Figure 8. Normalized TL curves of $Sr_2Si_5N_8$:0.02Eu^{2+} and $Sr_2Si_5N_8$:0.02Eu^{2+},0.02Dy^{3+}.

position of the emission peak with temperature are shown in Figure 9b. The emission peak displays a slight blue shift (from 622 to 618 nm) with the increasement of temperature. This temperature-induced blue shift can be explained by the thermally active phonon assisted excitation from low to high energy sublevels in the excited state of Eu^{2+} [41, 42, 43]. It is notable that the prepared $Sr_2Si_5N_8$:0.02Eu^{2+},0.02Dy^{3+} phosphor exhibits anomalous temperature-dependent photoluminescence property. The relative emission intensity of the sample is 105 % and 103 % of the initial value at 50 °C and 100 °C, respectively. The increase in emission intensity with increasing temperature is supposed to be caused by the difference in luminescence efficiency of the two emission centers (Eu_I and Eu_{II}) [43]. The emission centers at the short wavelength side are more sensitive in this process, which also coincides with the blue shift phenomenon described above. Remarkably, the relative emission intensity of the sample remains 98 % of the initial value at 150 °C. This excellent thermal stability material is highly suitable for optical information storage and white light-emitting diodes (LEDs) applications.

In addition, the chemical stability of $Sr_2Si_5N_8$:0.02Eu^{2+},0.02Dy^{3+} to humidity is explored using the scheme in Figure 10a. Figure 10b shows the luminescence of the samples under UV excitation after 0–7 (left to right) days of immersion in deionized (DI) water and the variation in luminescence intensity with immersion time is shown in Figure 10c. The luminescence intensity of the $Sr_2Si_5N_8$:0.02Eu^{2+},0.02Dy^{3+} phosphor remains almost unchanged after soaking in DI water for 7 days and drying at 60 °C. This excellent chemical stability provides security for efficient optical information storage applications.

A possible energy transfer process from Dy^{3+} ions to Eu^{2+} ions in $Sr_2Si_5N_8$ lattice is illustrated in Figure 11. Under the excitation of 345 nm and 370 nm, the electrons of Dy^{3+} ions can absorb the corresponding energy and be excited from ground state to $^6P_{7/2}$ and $^6P_{5/2}$ states, from which they subsequently relax to the $^4F_{9/2}$ level through non-radiative transitions and then return to the ground states ($^6H_{13/2}$ and $^6H_{15/2}$ levels) to produce the blue and yellow emissions. When Dy^{3+} and Eu^{2+} are co-doped in $Sr_2Si_5N_8$ lattice, part of the excited electrons in $^4F_{9/2}$ level transfer the energy to Eu^{2+} activators and subsequently decay to the ground state of $4f^7$ level. Finally, the Dy^{3+} and Eu^{2+} co-doped phosphor can generate red emission band at 630 nm owing to the $4f^65d^1 \rightarrow 4f^7$ transition of Eu^{2+} ions. Furthermore, the red emission of SSN:0.02Eu^{2+},0.02Dy^{3+} phosphor presents a higher photoluminescence intensity than Eu^{2+} singly-doped $Sr_2Si_5N_8$ phosphor, ascribed to the energy transfer from Dy^{3+}.

3.3. Application of optical information storage

Figure 12 presents the write-in and readout process of optical information storage for SSN:0.01Eu^{2+},0.02Dy^{3+} (I), SSN:0.02Eu^{2+},0.02Dy^{3+} (II), SSN:0.02Eu^{2+} (III), SSN:0.03Eu^{2+},0.02Dy^{3+} (IV) and SSN:0.05Eu^{2+},0.02Dy^{3+} (V) phosphors. As shown in Figure 12a, the specific photographic pattern (such as “apple” pattern) is recorded by covering a photomask on SSN:Eu^{2+},Dy^{3+} pellets under excitation of UV light during Step 1.

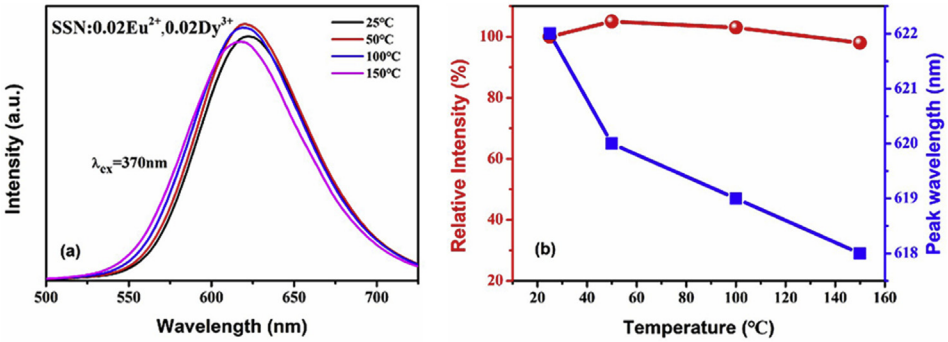

Figure 9. (a) Temperature-dependent PL spectra of $Sr_2Si_5N_8$:0.02Eu^{2+},0.02Dy^{3+} phosphor under 370 nm excitation. (b) Temperature dependence of relative emission intensity and emission peak position.

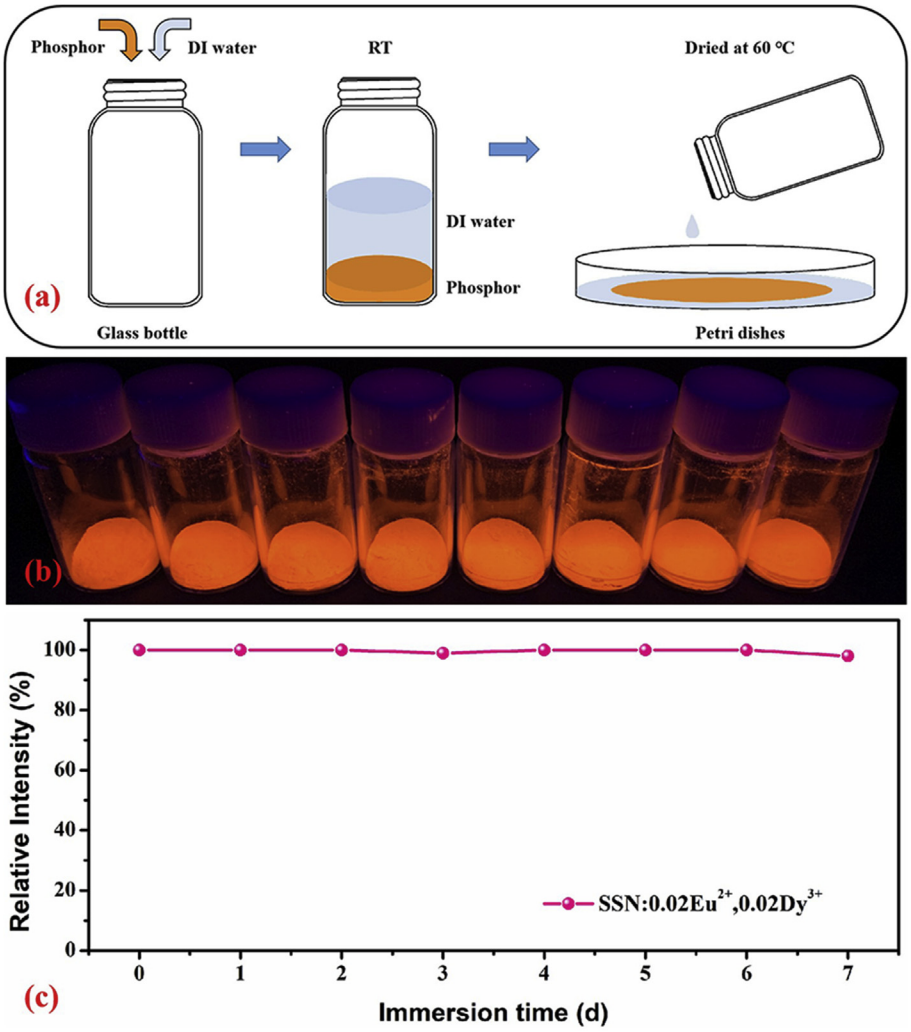

Figure 10. (a) Schematic diagram of the experimental procedure for chemical stability against humidity. (b) Image of samples under UV after 0–7 days of immersion in DI water. (c) Luminescence intensity of $Sr_2Si_5N_8$:0.02Eu^{2+},0.02Dy^{3+} as a function of immersion time.

After removing the photomask and UV excitation (Step 2), the optical information can be retrieved by heating the pellets to 100 °C or 200 °C. In Figure 12b, the "apple" pattern information is stored on the surface of SSN:0.01Eu^{2+},0.02Dy^{3+} (I), SSN:0.02Eu^{2+},0.02Dy^{3+} (II), SSN:0.02Eu^{2+} (III), SSN:0.03Eu^{2+},0.02Dy^{3+} (IV) and SSN:0.05Eu^{2+},0.02Dy^{3+} (V) phosphors through UV irradiation. After removal of the excitation source, the "apple" pattern is firstly preserved for 60 s due to the long-persistent phosphorescence. When the afterglow totally disappeared, the five phosphors are heated to 200 °C and the pattern of apple is read out for Dy^{3+} and Eu^{2+} co-doped phosphors. At 200 °C, the luminescence intensity of SSN:0.01Eu^{2+},0.02Dy^{3+} (I), SSN:0.02Eu^{2+},0.02Dy^{3+} (II), SSN:0.03E-u^{2+},0.02Dy^{3+} (IV) and SSN:0.05Eu^{2+},0.02Dy^{3+} (V) phosphors reached the

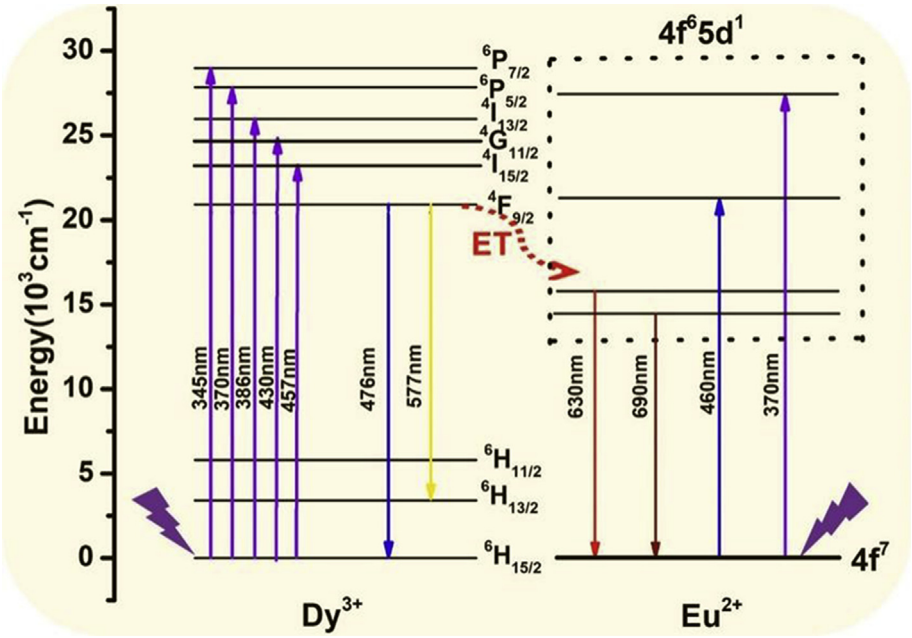

Figure 11. Energy level scheme of Dy^{3+} and Eu^{2+} ions in $Sr_2Si_5N_8$ lattice for the energy transfer process.

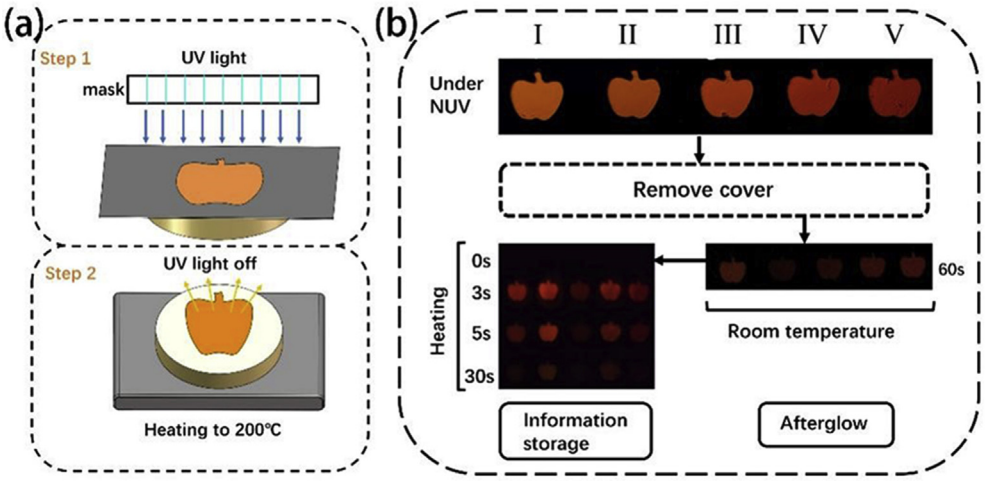

Figure 12. (a) Scheme mechanism of optical information storing process for $Sr_2Si_5N_8$:xEu^{2+},yDy^{3+} phosphors. (b) Write-in and readout of apple pattern for $Sr_2Si_5N_8$:xEu^{2+},yDy^{3+} phosphors (I) x = 0.01, y = 0.02 (II) x = 0.02, y = 0.02 (III) x = 0.02, y = 0 (IV) x = 0.03, y = 0.02 (V) x = 0.05, y = 0.02.

maximum at the fifth second, then decreased gradually until it disappeared 30 s later. However, it is obvious that the apple pattern for Eu^{2+} singly-doped phosphor (sample III in Figure 12b) never reappears after thermal stimulation. Therefore, Dy^{3+} ions could act as the trapping centers and are crucial to the optical information storage properties of the nitride phosphors.

Figure 13 displays the flexible PDMS luminescence film containing 20 wt% $Sr_2Si_5N_8$:0.02Eu^{2+},0.02Dy^{3+} phosphor and its optical information storage process. Figure 13a exhibits the fabricated flexible PDMS film with the sizes of 2.1 cm × 1.8 cm and 1/5 thickness of coin. The specific information pattern "DL" is stored on the flexible PDMS film by a "DL" photomask and UV irradiation, as depicted in Figure 13b. The PDMS film is subsequently pasted on a cup and the desired "DL" pattern clearly appears when filling the cup with boiling water (~100 °C). The curved and irregular surfaces of PDMS film with red-emitting persistent luminescence materials is expected to be huge applications in multidimensional optical information storage and medical imaging, especially for warning signal at high temperature.

In order to further expand optical information storage application on the surface of various materials, screen-printing process is used to fabricate the flexible luminescence film (Figure 14). Polypropylene polymer (PP) is used as the substrate material because of its favorable flexibility and heat resistance (up to 150 °C). As shown in Figure 14a, the phosphor film with enough flexibleness is formed on the frosted surface of PP material by screen printing process. Under excitation of UV light (254 nm), PP luminescence film generates red emission in Figure 14b and is covered by a photomask with a musical note pattern under UV light for 3 min to record the musical note pattern information (ii in Figure 14b). In process iii of Figure 14b, the musical note pattern stored on the flexible PP film is effectively released by a commercial 980 nm laser devices and the red emission area with note pattern can be observed. Excitingly, the i–iii processes of optical information storage are also achieved in Figure 14c using a blue light at 450 nm to excite the PP luminescence film, which has been placed on a heated platform at 200 °C for 3 min to empty the traps. The blue background in Figure 14c(ii) is due to visible light in the 450 nm band being captured by the camera while exciting the

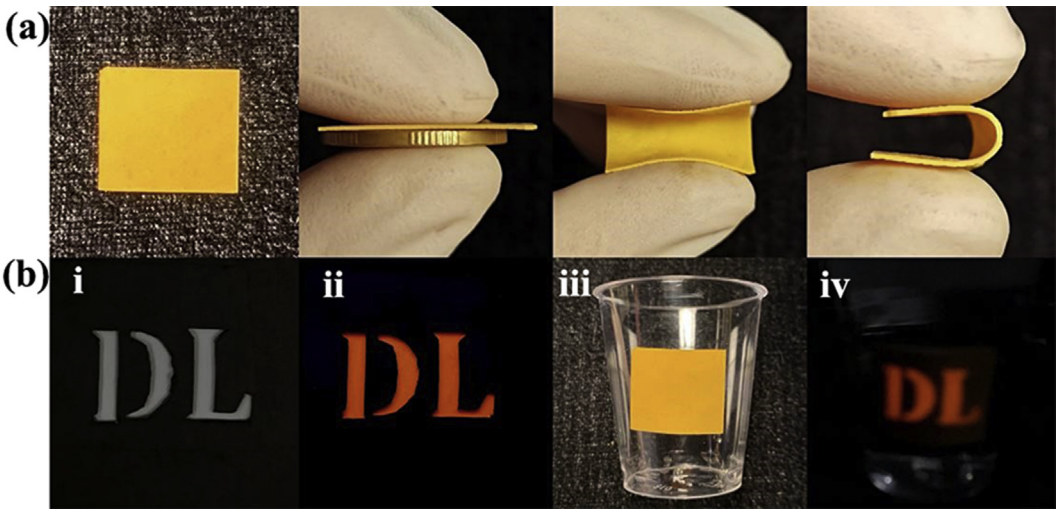

Figure 13. (a) Images of the flexible PDMS luminescence film with the thickness of ~0.4 mm fabricated by spin-coating process. (b) (i) Photomask of "DL" pattern; (ii) UV irradiation on the PDMS film; (iii) Removing UV excitation source and pasting the PDMS film on a cup; (iv) Readout of the "DL" pattern when filling the cup with boiling water (~100 °C).

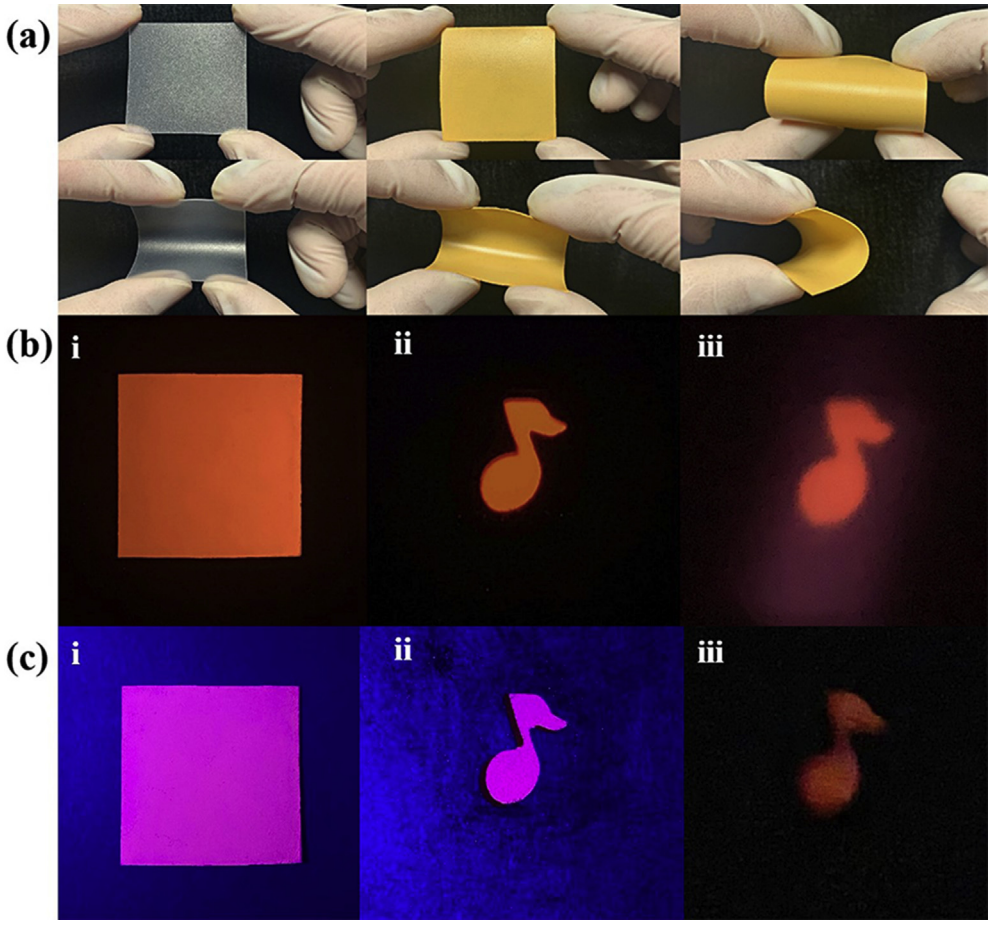

Figure 14. (a) Images of the flexible polypropylene (PP) luminescence film fabricated by screen printing process. (b) i: PP luminescence film with red emission under excitation of 254 nm ii: Covering the film by a photomask with a musical note pattern under UV light for 3 min iii: Retrieve of the musical note pattern by 980 nm laser. (c) i: PP luminescence film under excitation of 450 nm ii: Covering the film by a photomask with a musical note pattern under 450 nm light for 3 min iii: Retrieve of the musical note pattern by 980 nm laser.

PP luminescence film, whereas UV light belongs to the invisible light region and could not be captured by the camera in Figure 14b(ii). The clever combination of blue light and the red light emitted by the PP luminescence film allows the naked eye to recognize a different kind of purple information. The much weaker emission of panels iii under NIR stimulation after charging with blue light compared to UV is due to the fact that UV light excites the PP luminescence film more effectively and more photons are trapped in the same irradiation time, as can be seen from the excitation spectrum. This discovery raises new possibilities for the application of optical information storage. Obviously, the screen-printing technology and photo-stimulation of 980 nm further provide possible optical information storage applications on the surface of

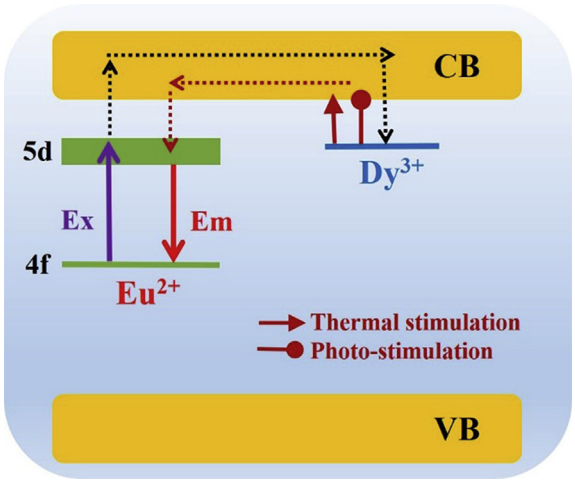

Figure 15. Schematic illustration of optical information storing mechanism.

different materials and room temperature environment, e.g. wearable devices.

3.4. Mechanism of thermal and photo-stimulated luminescence

A possible mechanism of optical information storing process for $Sr_2Si_5N_8:Eu^{2+},Dy^{3+}$ phosphors is proposed in Figure 15 based on the above results. Under near ultraviolet (NUV) excitation, electrons in 4f ground state of Eu^{2+} ions are excited to the high energy level of 5d states or the conduction band (CB). For Eu^{2+} singly-doped phosphor, the electrons subsequently relax to the lowest excited level of $4f^7 5d^1$ and red emission can be achieved due to 5d - 4f transition of Eu^{2+} ions. Whereas, the Dy^{3+} and Eu^{2+} co-doped phosphor has the trapping centers (Dy^{3+} ions) to capture the excited electrons in conduction band. After removal of UV excitation, the electrons stored in trap level of Dy^{3+} can jump back to the conduction band by thermal stimulation or photo-stimulation, and subsequently migrate to 5d state of Eu^{2+} ions. Finally, those electrons relaxed to the lowest level of 5d and return to 4f ground state and retrieve the stored optical information by photon emission.

4. Conclusions

In summary, the novel flexible luminescence films with unique with temperature and infrared response are successfully fabricated *via* screen printing and spin-coating technologies based on Eu^{2+}/Dy^{3+} co-doped $Sr_2Si_5N_8$ phosphors. Significant red luminescence by thermal or 980 nm stimulation can be obtained and used in full-color optical information storage. The co-doping of Dy^{3+} is vital to the photoluminescence properties of $Sr_2Si_5N_8$ based red emitting materials. It is obvious that Dy^{3+} singly-doped $Sr_2Si_5N_8$ phosphors exhibit similar crystal structure of $Sr_2Si_5N_8$ based on XRD patterns. Under excitation at 345 nm, the two emission peaks at 577 nm and 480 nm are observed for $Sr_2Si_5N_8:Dy^{3+}$ phosphors, the yellow emission at 577 nm corresponding to the $^4F_{9/2} \rightarrow {}^6H_{13/2}$ transition is prominent due to the low-symmetry local sites. Compared with $Sr_2Si_5N_8:0.02Eu^{2+}$ phosphor, the PL intensity of $SSN:0.02Eu^{2+},0.02Dy^{3+}$ phosphor is enhanced by 27 % for the red emission at 622 nm under NUV excitation at 370 nm, probably originating from the energy transfer from Dy^{3+} to Eu^{2+} ions. Interestingly, the prepared $SSN:0.02Eu^{2+},0.02Dy^{3+}$ phosphor can capture electrons through the trap center of Dy^{3+} and release photon emission through Eu^{2+} activator. Therefore, the PDMS and PP flexible films fabricated on the basis of $SSN:0.02Eu^{2+},0.02Dy^{3+}$ phosphor present write-in and read-out properties of desirable red luminescence, indicating its potential application in full-color optical information storage. Finally, a possible mechanism of optical information storing process is proposed for $SSN:Eu^{2+},Dy^{3+}$ phosphors.

Declarations

Author contribution statement

Hao Song: Conceived and designed the experiments; Performed the experiments; Analyzed and interpreted the data; Wrote the paper.

Xiuping Wu: Conceived and designed the experiments; Analyzed and interpreted the data; contributed reagents, materials, analysis tools or data; Wrote the paper.

Yanjie Zhang: Conceived and designed the experiments; Analyzed and interpreted the data; Wrote the paper.

Shichang Xu: Analyzed and interpreted the data; Wrote the paper.

Bing Li: Analyzed and interpreted the data; Contributed reagents, materials, analysis tools or data.

Funding statement

The work was financially supported by the National Natural Science Foundation of China (No. 82171883), the Shanxi Provincial Key Research and Development Project (202102130501002), the General Project of Liaoning Provincial Education Department (J2020067) and the Open Fund of Shanxi Province Key Laboratory of Oral Diseases Prevention and New Materials (KF2020-03).

Data availability statement

Data included in article/supplementary material/referenced in article.

Declaration of interests statement

The authors declare no conflict of interest.

Additional information

No additional information is available for this paper.

References

[1] M. Gu, Q. Zhang, S. Lamon, Nanomaterials for optical data storage, Nat. Rev. Mater. 1 (12) (2016), 16070.

[2] X. Chen, Y. Zhou, V. Roy, S.T. Han, Evolutionary metal oxide clusters for novel applications: toward high-density data storage in nonvolatile memories, Adv. Mater. 30 (3) (2018) 1703950.1–1703950.9.

[3] T. Wang, X. Ji, Z. Tao, X. Zhou, Z. Hao, X. Wang, X. Gao, S. Wang, Y. Liu, Dual stimuli-responsive lanthanide-based phosphors for an advanced full-color anti-counterfeiting system, RSC Adv. 10 (2020) 15573–15578.

[4] D. Liu, L. Yuan, Y. Jin, H. Wu, Y. Hu, Tailoring multidimensional traps for rewritable multilevel optical data storage, ACS Appl. Mater. Interfaces 11 (38) (2019) 35023–35029.

[5] R. Nicolas, X. Pan, B. Kate, R. Yinlan, T.M. Monro, J. Zhao, E.H. Heike, R. Hans, Towards rewritable multilevel optical data storage in single nanocrystals, Opt Express 26 (9) (2018) 12266–12276.

[6] Y. Zhuang, D. Chen, W. Chen, W. Zhang, R.J. Xie, X-ray-charged bright persistent luminescence in $NaYF_4:Ln^{3+}$@NaYF4 nanoparticles for multidimensional optical information storage, Light Sci. Appl. 10 (1) (2021) 132.

[7] Y. Zhuang, Y. Lv, L. Wang, W. Chen, T. Zhou, T. Takeda, N. Hirosaki, R.J. Xie, Trap depth engineering of $SrSi_2O_2N_2:Ln^{2+},Ln^{3+}$ (Ln^{2+} = Yb, Eu; Ln^{3+} = Dy, Ho, Er) persistent luminescence materials for information storage applications, ACS Appl. Mater. Interfaces 10 (2) (2018) 1854–1864.

[8] N. Majewska, T. Lesniewski, S. Mahlik, M. Grinberg, M. Sopicka-Lizer, Study of persistent luminescence and thermoluminescence in $SrSi_2N_2O_2:Eu^{2+},M^{3+}$ (M = Ce, Dy, Nd), Phys. Chem. Chem. Phys. 22 (30) (2020) 17152–17159.

[9] W. Liang, Y. Zhang, S. Xu, Structure and photoluminescence properties of Dy^{3+} doping in Sr-Si-O-N frameworks for highly efficient white light and optical information storage applications, Opt. Mater. 95 (9) (2019) 109250.1–109250.7.

[10] L. Yang, D.C. Zhu, S. Liu, J.S. Wang, C. Zhao, Y. Pu, Photoluminescence properties and crystal structure of $BaSiO_3:xEu^{3+},yBi^{3+}$ red phosphor synthesized by co-precipitation method, Phys. B Condens. Matter 556 (2018) 6–11.

[11] S. Katyayan, S. Agrawal, $CaSiO_3:Eu^{2+},Er^{3+}$, $BaSiO_3:Eu^{2+},Er^{3+}$ and $SrSiO_3:Eu^{2+},Er^{3+}$ phosphors: molten salt synthesis, optical and thermal studies, J. Mater. Sci. Mater. Electron. 31 (1) (2020) 8472–8480.

[12] G.J. Hoerder, M. Seibald, D. Baumann, T. Schröder, S. Peschke, P.C. Schmid, T. Tyborski, P. Pust, I. Stoll, M. Bergler, $Sr[Li_2Al_2O_2N_2]:Eu^{2+}$—a high performance red phosphor to brighten the future, Nat. Commun. 10 (1) (2019) 1824.

[13] G. Annadurai, B. Devakumar, H. Guo, R. Vijayakumar, B. Li, L. Sun, X. Huang, W. Kai, W.S. Xiao, Novel Eu^{3+}-activated $Ba_2Y_5B_5O_{17}$ red-emitting phosphors for white LEDs: high color purity, high quantum efficiency and excellent thermal stability, RSC Adv. 8 (2018) 23323–23331.

[14] G. Xiao, B. Zhou, X. Fang, D. Yan, Room-temperature phosphorescent organic-doped inorganic frameworks showing wide-range and multicolor long-persistent luminescence, Research 2021 (36) (2021) 1–11, article 1707621.

[15] B. Shen, J. Xu, Q. Ma O, J. Zhong, Enhanced luminescence properties of $Ca_{1+x}Sr_{2x}Al_2O_6$: Eu^{3+} ($0 \leq x \leq 1$) red phosphors based on composition modulation, RSC Adv. 11 (2021) 12981–12989.

[16] J. Zhao, H. Gao, H. Xu, Z. Zhao, H. Bu, X. Cao, L. He, Z. Yang, J. Sun, Structure and photoluminescence of Eu^{3+} doped Sr_2InTaO_6 red phosphor with high color purity, RSC Adv. 11 (2021) 8282–8289.

[17] L. Liu, R.J. Xie, Y.N. Hirosaki, Y.Y. Li, Z.T. Takeda, C.N. Zhang, J. Li, X. Sunz, Crystal structure and photoluminescence properties of red-emitting $Ca_9La_{1-x}(VO_4)_7$: xEu^{3+} phosphors for white light-emitting diodes, J. Am. Ceram. Soc. 93 (12) (2010) 4081–4086.

[18] S. Singh, A. Srivastava, Structural and spectral studies of highly pure red-emitting $Ca_3B_2O_6$:Eu^{3+} phosphors for white light emitting diodes, J. Alloys Compd. 869 (2021), 159363.

[19] C. Zhang, T. Uchikoshi, R.-J. Xie, L. Liu, Y. Cho, Y. Sakka, N. Hirosaki, T. Sekiguchi, Reduced thermal degradation of the red-emitting $Sr_2Si_5N_8$:Eu^{2+} phosphor via thermal treatment in nitrogen, J. Mater. Chem. C 3 (2015) 7642–7651.

[20] S. Hasegawa, T. Hasegawa, W.K. Sun, R. Yamanashi, M. Sato, Single crystal growth and crystal structure analysis of novel orange-red emission pure nitride $CaAl_2Si_4N_8$:Eu^{2+} phosphor, ACS Omega 4 (6) (2019) 9939–9945.

[21] H.C. Lin, C.Y. Yang, S. Das, C.H. Lu, Red-emission improvement of Eu^{2+}-Mn^{2+} co-doped $Sr_2Si_5N_8$ phosphors for white light-emitting diodes, Ceram. Int. 40 (8) (2014) 12139–12147.

[22] C.W. Yeh, W.T. Chen, R.S. Liu, S.F. Hu, H.S. Sheu, J.M. Chen, H.T. Hintzen, Origin of thermal degradation of $Sr_{2-x}Si_5N_8$:Eu_x phosphors in air for light-emitting diodes, J. Am. Chem. Soc. 134 (34) (2012) 14108–14117.

[23] Y.Q. Li, J. Steen, J. Krevel, G. Botty, A. Delsing, F.J. Disalvo, G.D. With, H.T. Hintzen, Luminescence properties of red-emitting $M_2Si_5N_8$:Eu^{2+} (M = Ca, Sr, Ba) LED conversion phosphors, J. Alloys Compd. 417 (1-2) (2006) 273–279.

[24] Zhang Wentao, Wang Yulong, Gao Yang, Long Jianping, Junfeng, Li, Sol–gel assisted synthesis and photoluminescence property of $Sr_2Si_5N_8$:Eu^{2+},Dy^{3+} red phosphor for white light emitting diodes, J. Alloys Compd. 667 (2016) 341–345.

[25] H. Zhang, Z. Cheng, Y. Zhang, Z. Hu, J. Yu, N. Zou, Improved luminescence properties and thermal stability of $SrSi_2O_2N_2$:Eu^{2+} phosphor with single phase via the formation of Eu^{3+} on surface structure, J. Mater. Sci. 52 (12) (2017) 7605–7614.

[26] Weiler Volker, Pust Philipp, Hecht Cora, Narrow-band red-emitting $Sr[LiAl_3N_4]$:Eu^{2+} as a next-generation LED-phosphor material, Nat. Mater. 13 (9) (2014) 891–896.

[27] Y. Lan, D. Wang, D. Xie, J. Tan, B. Li, M. Zhang, Y. Chen, Preparation of red phosphor $Sr_2Si_5N_8$: Eu^{2+} by pellet method and its optical characteristics, Coatings 11 (3) (2021) 283.

[28] T. Horikawa, X.Q. Piao, M. Fujitani, H. Hanzawa, K. Machida, Preparation of $Sr_2Si_5N_8$:Eu^{2+} phosphors using various novel reducing agents and their luminescent properties, IOP Conf. Ser. Mater. Sci. Eng. 1 (1) (2009), 012024.

[29] K.S. Choi, S.D. Jee, J.P. Lee, C.H. Kim, A novel synthetic method of $Sr_2Si_5N_8$:Eu^{2+} from $SrSi_2O_2N_2$:Eu^{2+} by carbo-thermal reduction and nitridation, J. Nanosci. Nanotechnol. 13 (3) (2013) 1867–1870.

[30] X. Peng, L.I. Shu-Xing, X.J. Liu, Z.R. Huang, L.I. Hui-Li, Syntheses and photoluminescence properties of $Sr_2Si_5N_8$:Eu^{2+} phosphors, J. Inorg. Mater. 29 (12) (2014) 1281–1286.

[31] H. Zhang, H. Dong, B. Lei, P. Wang, J. Li, Y. Liu, J. Wang, Y. Xiao, M. Zheng, J. Meng, Enhanced performance of $Ca_2Si_5N_8$:Eu^{2+},Tm^{3+} reddish-orange afterglow phosphor by co-doping with Dy^{3+}, Opt. Mater. 36 (11) (2014) 1846–1849.

[32] J. Li, B. Lei, J. Qin, Y. Liu, X. Liu, Temperature-dependent emission spectra of $Ca_2Si_5N_8$:Eu^{2+}, Tm^{3+} phosphor and its afterglow properties, J. Am. Ceram. Soc. 96 (3) (2013) 873–878.

[33] Z. Ma, J. Zhou, J. Zhang, S. Zeng, H. Zhou, A.T. Smith, W. Wang, L. Sun, Z. Wang, Mechanics-induced triple-mode anticounterfeiting and moving tactile sensing by simultaneously utilizing instantaneous and persistent mechanoluminescence, Mater. Horiz. 6 (10) (2019) 2003–2008.

[34] Wen Qin, Yang Jinglian, Li SongRu, Gao Jinwei, Lu Xubing, Micropatterning of lanthanide complex species onto self-cracking flexible transparent films and their photophysical properties, Mater. Res. Bull. 88 (2017) 98–104.

[35] W. Zhang, Y. Lu, H. Du, J. Lin, J. Long, Sol-gel-nitridation preparation and photoluminescence properties of Dy^{3+}-doped $M_2Si_5N_8$ (M=Ca, Sr, Ba) phosphors for white light emitting diodes, Ceram. Int. 43 (1) (2017) 1080–1085.

[36] L. Bo, L. Kong, C. Shi, White-light long-lasting phosphor $Sr_2MgSi_2O_7$:Dy^{3+}, J. Lumin. 122–123 (1) (2007) 121–124.

[37] M. Jayasimhadri, B.V. Ratnam, K. Jang, H.S. Lee, B. Chen, S.S. Yi, J.H. Jeong, L.R. Moorthy, Greenish-yellow emission from Dy^{3+}-doped Y_2O_3 nanophosphors, J. Am. Ceram. Soc. 93 (2) (2010) 494–499.

[38] J.B. Gruber, B. Zandi, U.V. Valiev, S.A. Rakhimov, Energy levels of Dy^{3+} ($4f^9$) in orthoaluminate crystals, J. Appl. Phys. 94 (2) (2003) 1030–1034.

[39] T. Li, P. Li, Z. Wang, S. Xu, Q. Bai, Z. Yang, Coexistence phenomenon of Ce^{3+}-Ce^{4+} and Eu^{2+}-Eu^{3+} in Ce/Eu co-doped $LiBaB_9O_{15}$ phosphor: luminescence and energy transfer, Phys. Chem. Chem. Phys. 19 (5) (2017) 4131–4138.

[40] C. Wang, Y. Jin, Y. Lv, G. Ju, D. Liu, L. Chen, Z. Li, Y. Hu, Trap distribution tailoring guided design of super-long-persistent phosphor Ba_2SiO_4:Eu^{2+},Ho^{3+} and photostimulable luminescence for optical information storage, J. Mater. Chem. C 6 (22) (2018) 6058–6067.

[41] C.F. Varela, Y.D. Molina, S. Sandovalgutiérrez, L.C. Moreno-Aldana, C.A. Parravargas, Optical and structural properties of the Fe^{3+}-doped $Lu_3Al_5O_{12}$:Ce^{3+} garnet phosphor, RSC Adv. 11 (10) (2021) 11804–11812.

[42] Qin Chuanxiang, Huang Yanlin, Shi Liang, Chen Guoqiang, Qiao Xuebin, Thermal stability of luminescence of $NaCaPO_4$:Eu^{2+} phosphor for white-light-emitting diodes, J. Phys. Appl. Phys. 42 (18) (2009), 185105.

[43] Z. Xia, X. Wang, Y. Wang, L. Liao, X. Jing, Inorganic chemistry, synthesis, structure, and thermally stable luminescence of Eu^{2+}-doped $Ba_2Ln(BO_3)_2Cl$ (Ln = Y, Gd and Lu), Host Compd. 50 (20) (2011) 10134–10142.